# Urine metabolomics of rats with chronic atrophic gastritis

Urine metabolomics

Guo-Xiu Zu[1¶], Qian-Qian Sun[1¶], Jian-Chen[1,4¶], Xi-Jian Liu[1], Ke-Yun Sun[1], Liang-Kun Zhang[1], Ling li[1], Tao Han[2*], Ha I-Liang Huang[3*]

[1] Department of Traditional Chinese Medicine, Shandong University of Traditional Chinese Medicine, Jinan, Shandong, China

[2] Graduate Office ,Shandong University of Traditional Chinese Medicine, Jinan, Shandong, China

[3] Department of Rehabilitation Medicine, Shandong University of Traditional Chinese Medicine, Jinan, Shandong, China

[4]Affiliated Central Hospital of Shandong First Medical University,Shandong First Medical University, Jinan, Shandong, China

¶ These authors contributed equally to this work.

* Corresponding author

E-mail: 60012002@sdutcm.edu.cn (TH)

E-mail: 06000031@sdutcm.edu.cn (HH)

# Abstract

Background/Aim: To use liquid chromatography-mass spectrometry (LC-MS) to identify endogenous differential metabolites in the urine of rats with chronic atrophic gastritis (CAG). Materials and Methods: Methylnitronitrosoguanidine (MNNG) was used to produce a CAG model in Wistar rats, and HE staining was used to determine the pathological model. LC-MS was used to detect the differential metabolic profiles in rat urine. Diversified analysis was performed by the statistical method. Results: Compared with the control group, the model group had 68 differential metabolites, 25 that were upregulated and 43 that were downregulated. The main metabolic pathways were D-glutamine and D-glutamic acid metabolism, histidine metabolism and purine metabolism. Conclusion: By searching for differential metabolites and metabolic pathways in the urine of CAG rats, this study provides effective experimental data for the pathogenesis and clinical diagnosis of CAG.

# Introduction

Chronic atrophic gastritis (CAG) is a type of atrophy of gastric mucosal epithelial cells and glands where the number of glands is reduced, the mucosal layer thins, and the mucosal muscle layer thickens and may be accompanied by intestinal metaplasia and dysplasia. Digestive system diseases [1] mainly have the clinical manifestations of bloating, fullness of the stomach, belching, pain in the upper abdomen, loss of appetite, weight loss, etc. CAG has a wide variety of factors and is a common and frequently occurring clinical disease with a 2.55%- 7.46% canceration rate [2]. In 1978, the World Health Organization officially defined chronic atrophic gastritis as a precancerous state. The active treatment of CAG in clinical practice is an important node to block its development into gastric cancer.

As an important branch of systems biology, metabolomics technology is unique because it does not require the establishment of a large database of expressed gene sequences [3]. Metabolomics can express the physiological and biochemical state of the body through biological metabolic structure to better analyze pathogenesis. Among its advantages, liquid chromatography-mass spectrometry (LC-MS) technology can be directly used to analyze biological metabolites to obtain final analysis results with the advantage of finding subtle changes in gene and protein expression during biological metabolism. Thus, LC-MS has become the most commonly used analytical technique in metabolomics research [4]. This study explains the molecular mechanism of action and metabolic pathways of chronic atrophic gastritis through pharmacodynamics and LC-MS.

# Materials and methods

## *Animals*

Twenty SPF grade Wistar male rats, 6 weeks old, 180 ± 20 g, were provided by Shandong Pengyue Experimental Animal Co., Ltd. [SCXK (Lu) 20140007]. The feeding environment was a temperature of 26 °C ± 2 °C, humidity 50 ± 10%, and light illumination/dark cycle 12 h. The experiment started after 7 d of adaptive feeding from the time of purchase. During the period, the animals has free access to food and drinking water, and the experiment met animal ethical requirements.

## *Experimental reagents and instruments*

Methylnitronitrosoguanidine (manufactured by Tokyo Chemical Industry Co., Ltd., NH8JH-DR), vetzyme tablets (Lepu Hengjiuyuan Pharmaceutical Co., Ltd., 20170401), ranitidine hydrochloride capsules (Tianjin Pacific Pharmaceutical Co., Ltd., 20170601), and ammonium hydroxide (Shanghai Wokai Biotechnology Co., Ltd., 20170220) were used. Anhydrous ethanol (Tianjin Fuyu Fine Chemical Co., Ltd., 20170808), methanol (Woke), acetonitrile and formic acid (Aladdin), ammonium formate (Sigma), hematoxylin staining solution, eosin staining solution, differentiation solution, blue back solution (Hebei Bohai Biological Engineering Development

Co., Ltd.), and xylene (Tianjin Yongda Chemical Reagent Co., Ltd.) were also utilized in this study.

A refrigerated centrifuge (Eppendorf, H1650-W), mixer (Vortex Mixer, QL-866), liquid chromatograph (Thermo, UltiMate 3000) and mass spectrometer Thermo (Q Exactive Focus) were instruments used in this study.

## *Animal model*

Twenty Wistar rats were prepared, and 10 rats were randomly selected as a blank group. Normal diet was fed until the materials were collected. The remaining rats were model rats according to the following method [5]: rats were given 120 μg/mL MNNG from the 1st day of modeling, given 0.1% ammonia water freely for 24 h fed with 0.03% ranitidine feed using the hunger and satiety method (full food for 2 d, fasting for 1 d), an each given 2 ml of 40% ethanol on the fasting day. The above operation lasted for 16 weeks and each rat was weighed twice a week during the modeling process. During the experiment, the weight, coat color and behavior of the rats were observed.

## *Urine collection and preparation*

Before taking the material, the rats were fasted for 24 h while drinking water normally, and urine was collected from the rats. Urine was centrifuged at 2500 rpm at room temperature for 1 hour in the morning, and the supernatant was divided into centrifuge tubes; each tube was > 0.3

ml. The urine samples were melted at 4 °C and 100 μL of each sample was placed into a 1.5 mL centrifuge tube, 100 μL of dd$H_2O$ was added followed by shaking for 5 min to fully absorb and centrifugation at 10000 g and 4 °C for 10 min. Then, a 0.22 μm membrane was used to filter the supernatant to obtain the samples to be tested; 20 μL of the synthetic QC samples were extracted from each sample to be tested, and the remaining samples were tested by LC-MS.

## *LC-MS chromatographic mass spectrometry conditions*

A Thermo Ultimate 3000 chromatograph and an ACQUITY UPLC® HSS T3 1.8 μm (2.1 × 150 mm) chromatographic column were used with an autosampler temperature of 8 °C, a flow rate of 0.25 mL/min, and a column temperature of 40 °C. The sample was eluted with an injection volume of 2 μl, and the positive mode mobile phases were 0.1% formic acid in water (A) and 0.1% formic acid in acetonitrile (B). The gradient elution program was 0 ～ 2 min, 2% B; 2 ～ 10 min, 2% ～ 50% B; 10 ～ 15 min, 50% ～ 98% B; 15 ～ 20 min, 98% B; 20 ～ 22 min, 98% ～ 2% B; 22 ～ 25 min, 2% B. The negative mode mobile phases were 5 mM ammonium formate (A) and acetonitrile (B). The gradient elution program was 0 ～ 2 min, 2% B; 2 ～ 10 min, 2% ～ 50% B; 10 ～ 15 min, 50% ～ 98% B; 15 ～ 20 min, 98% B; 20 ～ 22 min, 98% ～ 2% B; 22 ～ 25 min, 2% B [6]. The Thermo Q Exactive Focus mass spectrometer was operated with the following conditions: electrospray ion (ESI) source, positive and negative ion ionization mode, positive ion spray voltage of 3.50 kV, negative ion spray voltage of -2.50 kV, sheath gas of 30 arb, auxiliary gas of 10 arb, capillary temperature of 325 °C, full scan with a resolution of 70,000, scan range of

m/z 81-1000, secondary cracking with HCD, collision voltage of 30 eV, and dynamic exclusion to remove unnecessary MS/MS information.

### *Data processing*

The obtained raw data was converted to mzXML format with ProteoWizard software (v3.0.8789) [7] and the RCMS (v3.3.2) XCMS package was used for peak identification, peak filtering, and peak alignment analysis. The main parameters were bw = 5, ppm = 15, peakwidth = c (10, 20), mzwid = 0.015, mzdiff = 0.01, and method = centWave, which includes the mass to charge ratio (m/z) and information data matrix such as retention time (rt) and intensity.

## Results

### *General situation*

Control group: In good condition, sturdy body, strong limbs, neat, supple and shiny fur, mental state is excellent, responsive to external conditions, body weight gradually increases, and the stool is normal. Model group: Poor condition, thin body, weak limbs, messy fur, dryness, and dullness, poor mental state, drowsiness, unresponsive to external conditions, insignificant changes in body mass, slower rise, and less stool that is hard. Body mass changes are shown in Fig. 1.

**Fig. 1. Mass Variation Diagram of the Control Group and Model Group.**

## *Observation of pathological tissues*

As shown in Fig. 2A, the gastric tissue mucosa lamina propria in the blank group pathological section is rich in gastric glands that are closely arranged with a normal structure, and the gastric gland epithelial cells have a normal morphology. In the model group, the lamina propria were loosely arranged, the lamina propria of the gastric mucosa was severely congested (black arrow), and there were a large number of inflammatory cells (blue arrow) under the mucosa with edema, as shown in Fig. 2B.

**Fig. 2. HE Staining Pathological Sections.** A. HE Staining Pathological Sections of Gastric Mucosa in the Control Group (×200); 2-B: HE Staining Pathological Sections of Gastric Mucosa in the Model Group (×200).

## *Chromatogram in total ion mode*:

The components separated by chromatography entered into mass spectrometry (MS) analysis, and data collection was performed by continuous scanning of the mass spectrum. The intensity is on the ordinate, and the time is on the abscissa. The resulting spectrum is the base peak chromatogram (BPC); see Fig. 3A and B (G: model group, H: control group)

**Fig. 3. Chromatogram in Total Ion Mode**. 3-A: Typical Sample BPC in Positive Ion Mode, 3-B: Typical Sample BPC in Negative Ion Mode.

## *Urine metabolomics analysis in positive ion mode*

CAG urine metabolomics analysis is corrected positive ion data. After the data were preprocessed, the principal component analysis (PCA) method was used to explore CAG urine in positive ion mode. Changes in the fluid metabolism profile yielded a model with three principal components (R2 = 0.548) and a score chart reflecting the degree of dispersion between groups, as shown in Fig. 4A. The PCA score graph shows that most samples are within the ellipse of the 95% confidence interval except for individual outliers. The PCA score graph shows that the urine samples of the two groups are significantly separated and are statistically significant. Furthermore, PLS-DA and OPLS-DA analysis methods (Fig. 4B and C) were used to remove information that was not related to sample classification, and pattern discrimination analysis was performed on the full spectrum of the urine. The results showed that the two groups of samples could be significantly separated. In order to check whether the repeatability of the model is good and ensure the reliability of the data model, a permutation test was performed on the model (Fig. 4D). The above results show that the multivariate data model of urine samples meets the parameter standard, indicating that the model has high stability and good predictive ability.

**Fig. 4. Urine Metabolism Profile of CAG Model Rats in Positive Ion Mode.** 4-A: PCA Scores, 4-B: PLS-DA Scores, 4-C: OPLS-DA Scores, 4-D: Replacement Test of the CAG Model Urine Fit Model in Positive Ion Mode.

## *Analysis of urine metabolomics in negative ion mode*

The PCA method was used to explore changes in the CAG urine metabolic spectrum. After data preprocessing, a model with 3 principal components (R2 = 0.515) and the degree of dispersion between groups were obtained from the score chart. The PCA score graph shows that most samples fall within the ellipse of the 95% confidence interval, with only a few outliers. The PCA score (Fig. 5A) graph shows the spatial distribution of the urine samples of the two groups, which can be significantly separated. PLS-DA and OPLS-DA analysis methods were used to further analyze the full spectrum of urine, and the results showed that the two groups of samples could be significantly separated (Fig. 5B and C). In order to test whether the repeatability of the model is good and to ensure reliability of the data model, the model was replaced and verified (Fig. 5D). The intercept of Q2 is negative, indicating that the model is valid. The above results indicate that the multivariate data model of urine samples meets the parameter standard, indicating that the model has high stability and good predictive ability.

**Fig. 5. Urine Metabolism Profile of CAG Model Rats in Negative Ion Mode.** 5-A: PCA Scores, 5-B: PLS-DA Scores, 5-C: OPLS-DA Scores, 5-D: Replacement Test of the CAG Model Urine Fit Model in Negative Ion Mode.

## *Extraction and analysis of differential metabolites*

From the PCA, PLS-DA, OPLS-DA analysis model group and blank group, the screening conditions were in accordance with a P-value ≤0.05, VIP ≥1 [6], and molecular weight error <20 ppm). According to the fragmentation information obtained from MS/MS mode, further matching

192 annotations were obtained in the HMDB, METLIN, MassBank, LipidMaps, and mzCloud
193 databases to obtain accurate metabolite information. A total of 68 differential metabolites were
194 screened, of which 25 were upregulated and 43 that were downregulated, compared with
195 metabolites with the same or similar metabolic modes clustered to obtain differential metabolite
196 heat maps and metabolite correlation heat maps (Fig. 6). These differential metabolites relied on
197 the Marker-view, KEGG, HMDB, MetaboAnalyst and other databases, which were searched and
198 identified, and the results are shown in Table 1.

199 **Fig. 6. Heat Map of the Differential Metabolites.** A: Heat Map of the Differential Metabolites
200 in CAG Rats; 6-B: Correlation Heat Map of Differential Metabolites in CAG Rats.

201 **Table 1. Differential Metabolic Markers in Urine of CAG Rats (Upregulated ↑,**
202 **Downregulated ↓).**

| chemical compound | chemical formula | Model vs Control_VIP | log2 (FC) | p value |
|---|---|---|---|---|
| Arbutin | C12H16O7 | 1.771574784 | 2.3461 | 0.012648447↑ |
| Inosine | C10H12N4O5 | 1.528975498 | 2.1558 | 0.037258488↑ |
| Adenosine | C10H13N5O4 | 1.934286006 | 2.0713 | 0.004285334↑ |
| 5-S-Methyl-5-thioadenosine | C11H15N5O3S | 2.284849647 | 1.8528 | 0.000234115↑ |
| 10-Hydroxy capric acid | C10H20O3 | 1.823597606 | 1.5684 | 0.008306808↑ |
| 7-Methylguanosine | C11H16N5O5 | 1.568140916 | 1.549 | 0.031843615↑ |
| Pipecolic acid | C6H11NO2 | 1.781759339 | 1.5181 | 0.010438908↑ |
| delta-Decalactone | C10H18O2 | 1.849847045 | 1.5177 | 0.007156206↑ |

| | | | | |
|---|---|---|---|---|
| 3-Methyl-L-histidine | C7H11N3O2 | 1.872481394 | 1.4212 | 0.00738418↑ |
| Dihydro-3-coumaric acid | C9H10O3 | 1.528214666 | 1.394 | 0.037370134↑ |
| Adipic acid | C6H10O4 | 2.113128751 | 1.3866 | 0.001516902↑ |
| 2-Methylguanosine | C11H15N5O5 | 1.751775025 | 1.367 | 0.012215874↑ |
| Guanosine | C10H13N5O5 | 1.53671651 | 1.3507 | 0.032900583↑ |
| Suberic acid | C8H14O4 | 1.612701672 | 1.3484 | 0.026434225↑ |
| 2-Deoxycytidine | C9H13N3O4 | 1.915004809 | 1.3307 | 0.004840515↑ |
| D-Glucuronic acid | C6H10O7 | 2.241280415 | 1.2756 | 0.000512579↑ |
| CMPF | C12H16O5 | 2.124552651 | 1.2416 | 0.001388456↑ |
| Gentisic acid | C7H6O4 | 1.835909917 | 1.2406 | 0.009038573↑ |
| TMCA | C12H14O5 | 1.954028191 | 1.161 | 0.003771041↑ |
| 2-Aminopteridine-4,7-Diol | C6H5N5O2 | 2.016289866 | 1.1144 | 0.003043425↑ |
| 4-Hydroxy nonenal Mercapturic acid | C14H25NO5S | 1.548812817 | 1.0965 | 0.034435408↑ |
| D-Biotin | C10H16N2O3S | 1.515098427 | 1.0857 | 0.035928770↑ |
| N-Acetylcadaverine | C7H16N2O | 1.640234776 | 1.0602 | 0.020995681↑ |
| Benzaldehyde | C7H6O | 1.762739968 | 1.0398 | 0.011540491↑ |
| Guanidinoacetic acid | C3H7N3O2 | 1.705152566 | 1.0027 | 0.015441198↑ |
| 3-Methylindole | C9H9N | 1.876426797 | 0.9857 | 0.007221167↓ |
| 2-Oxoglutaric acid | C5H6O5 | 1.495118055 | 0.9552 | 0.042475723↓ |
| Marmesin acetate | C16H16O5 | 1.720421852 | 0.9461 | 0.014319362↓ |

| | | | | |
|---|---|---|---|---|
| N-Lactoyl-phenylalanine | C12H15NO4 | 1.57132921 | 0.907 | 0.028460454↓ |
| Taxifolin | C15H12O7 | 1.718717369 | 0.8785 | 0.016387198↓ |
| 3-(3,4-Dihydroxyphenyl)Propanoic acid | C9H10O4 | 2.070984986 | 0.8642 | 0.002077192↓ |
| N(2)-Acetyl-L-Lysine | C8H16N2O3 | 2.049816081 | 0.8419 | 0.001930407↓ |
| L-Phenylalanyl-L-Proline | C14H18N2O3 | 2.077282892 | 0.7931 | 0.001566615↓ |
| O-Toluic acid | C8H8O2 | 1.805758215 | 0.7836 | 0.009169037↓ |
| Quinaldic acid | C10H7NO2 | 1.669168777 | 0.7797 | 0.020624237↓ |
| 3-Hydroxy-3-methylglutaric acid | C6H10O5 | 1.480741362 | 0.7542 | 0.044849483↓ |
| Dopamine | C8H11NO2 | 1.825498392 | 0.753 | 0.008218865↓ |
| Syringic acid | C9H10O5 | 1.538159222 | 0.7057 | 0.035930624↓ |
| N-Acetyl-Glutamic acid | C7H11NO5 | 1.606367357 | 0.6886 | 0.024447196↓ |
| N,N-Diethyl-M-Toluamide | C12H17NO | 1.658473782 | 0.6825 | 0.019299997↓ |
| N-epsilon-Acetyl-L-lysine | C8H16N2O3 | 2.024611789 | 0.6354 | 0.00287668↓ |
| Glutaric acid | C5H8O4 | 1.55606035 | 0.6234 | 0.033445496↓ |
| 3-Indoleacetic acid | C10H9NO2 | 1.490647745 | 0.5842 | 0.043203485↓ |
| Homovanillic acid | C9H10O4 | 1.602561332 | 0.5841 | 0.027598265↓ |
| L-Histidine | C6H9N3O2 | 1.603838417 | 0.5723 | 0.024721392↓ |
| Hexanoylcarnitine | C13H25NO4 | 1.466692106 | 0.5425 | 0.043469353↓ |
| Nonic acid | C9H16O4 | 2.208499912 | 0.5276 | 0.000690754↓ |
| 4-Acetamidobutanoic acid | C6H11NO3 | 1.641325837 | 0.526 | 0.02089112↓ |

| | | | | |
|---|---|---|---|---|
| N-Acetyl-beta-Alaninate | C5H9NO3 | 1.573650573 | 0.5139 | 0.028179966↓ |
| (S)-2-Hydroxyglutarate | C5H8O5 | 1.464880663 | 0.5013 | 0.047581863↓ |
| N-Acetyl-L-Histidine | C8H11N3O3 | 1.573531368 | 0.4979 | 0.028194318↓ |
| 2-Pyrrolidone-5-Carboxylic acid, Methyl Ester | C6H9NO3 | 1.868632508 | 0.4193 | 0.006413493↓ |
| 2-Hydroxypropanoic acid | C3H6O3 | 1.874058772 | 0.3997 | 0.00731866↓ |
| 3-Hydroxycapric acid | C10H20O3 | 1.944065438 | 0.3836 | 0.004843594↓ |
| ®-Noradrenaline | C8H11NO3 | 1.526685758 | 0.3797 | 0.037595251↓ |
| Dacarbazine | C6H10N6O | 1.587732534 | 0.2827 | 0.026523445↓ |
| Phenacylamine | C8H9NO | 1.489849766 | -0.4527 | 0.039727046↓ |
| Threonate | C4H8O5 | 1.547635686 | -0.6082 | 0.034598259↓ |
| Adenine | C5H5N5 | 1.792987662 | -0.7032 | 0.011340028↓ |
| Dodecanedioic acid | C12H22O4 | 1.66119894 | -0.9546 | 0.021378107↓ |
| 2-Deoxyuridine | C9H12N2O5 | 1.943477192 | -0.979 | 0.004861136↓ |
| Formononetin | C16H12O4 | 2.025071834 | -1.1042 | 0.002867682↓ |
| L-Glutamic acid | C5H9NO4 | 1.777690879 | -1.1167 | 0.010667276↓ |
| Genkwanin | C16H12O5 | 2.062070851 | -1.1857 | 0.002214871↓ |
| Nicotinic acid | C6H5NO2 | 2.168087639 | -1.2801 | 0.000737259↓ |
| Guanine | C5H5N5O | 2.476437968 | -1.3203 | 3.25E-05↓ |
| Adenosine 3-monophosphate | C10H14N5O7P | 1.68169368 | -1.3227 | 0.019481197↓ |
| AMP | C10H14N5O7P | 1.900260783 | -1.5778 | 0.005302741↓ |

## *CAG model group urine differential metabolite pathway information*

This study mapped the differential metabolites to the KEGG database. There are 23 common metabolic pathways involved in the obtained differential metabolites, as shown in Fig. 7: D-glutamine and D-glutamine histidine metabolism, histidine metabolism, purine metabolism, nitrogen metabolism, tyrosine metabolism, arginine-proline metabolism, butyric acid metabolism, biotin metabolism, alanine-aspartic acid-glutamic acid metabolism, ascorbic acid-bitter almond metabolism, niacin-nicotinamide metabolism, pentose-glucuronate interconversion, pyrimidine metabolism, lysine degradation, citric acid cycle (TCA cycle), starch-sucrose metabolism, Inositol phosphate metabolism, glutathione metabolism, porphyrin and chlorophyll metabolism, cysteine-methionine metabolism, glycine-serine-threonine metabolism, aminoacyl-tRNA biosynthesis, and tryptophan metabolism. Among them, the metabolic pathways with * P <0.5 and Impact> 0 include D-glutamine and D-glutamic acid metabolism, histidine metabolism, and purine metabolism, as shown in Table 2.

**Fig. 7. Metabolic Pathways of CAG Rat Metabolites Mapped to KEGG.**

**Table 2. Differential Metabolic Pathways in Urine of CAG Rats**

| | | |
|---|---|---|
| D-Glutamine and D-glutamate metabolism | Histidine metabolism | Purine metabolism |

| | | | |
|---|---|---|---|
| p value | 0.013036 | 0.016826 | 0.039418 |
| Impact | 1 | 0.24194 | 0.076410 |
| constituent structures | 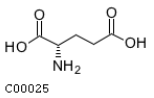 C00025 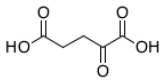 C00026 | 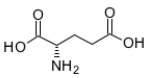 C00025 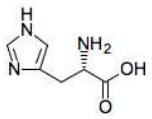 C00135 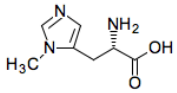 C01152 | 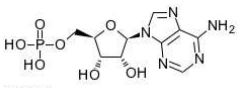 C00020  C00147 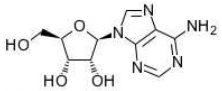 C00212 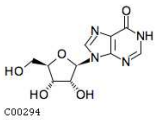 C00294 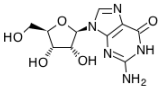 C00387 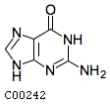 C00242 |
| Pathway links | http://www.kegg.jp/pathway/rno00471+C00025+C00026 | http://www.kegg.jp/pathway/rno00340+C00025+C00135+C01152 | http://www.kegg.jp/pathway/rno00230+C00020+C00212+C00294+C00242+C00387+C00147 |

# Discussion

Metabolomics is an emerging technology for different metabolic pathways of the products by stimulating or disturbing the differences in metabolites displayed by organisms. It can qualitatively, quantitatively and systematically study endogenous small molecules (including blood, urine, and the overall and dynamic laws of tissue fluids) and is widely used in the early diagnosis of diseases, biomarker discovery, pathogenesis research and pharmacological mechanism research. This technology has obvious integrity and dynamic characteristics consistent with the overall theory of traditional Chinese medicine. There is also great potential in explaining the pathogenesis of diseases [8]. Combining pattern recognition and other informatics methods can

be used to analyze the changes in metabolic products caused by physiological and pathological stimuli of organisms and genetic factors. PCA technology can reduce data dimensions and maintain original data, which can improve the detection of abnormal data. It cannot, however, ignore intragroup errors and eliminate random errors that are irrelevant to the content of the study, while PLS-DA and OPLS-DA can maximize the specified sample differences in the analysis, making it easier to find differential metabolic profiles. MetPA can find interfering metabolic pathways and establish a regression model through the commonly used data processing methods of topological analysis [9] and make a discriminant analysis of the regression results [10]. OPLS-DA makes the difference between groups on the basis of PLS-DA useful to help analyze related metabolic pathways [11]. Therefore, the combination of these four methods is a powerful tool for determining disease biomarkers. Comparing the expression of urine metabolites from the level of metabolomics and determining differential metabolites and metabolic pathways can provide an objective basis for the clinical diagnosis of CAG.

Liquid chromatography-mass spectrometry (LC-MS) is based on the principle of high-performance liquid chromatography (HPLC) adsorption combined with the analysis technique of the mass-to-charge ratio of charged particles. It is used to determine the mass of particles and determine the elemental composition of samples or molecules to elucidate the chemical structure of the molecule. Compared with other chromatographic methods, the LC-MS sample preparation time is short, has high selectivity, and is not affected by chromatographic resolution. It can carry out the structural analysis of compounds to identify known and unknown compounds and can

249 quickly identify and elute metabolites. Analysis, through limited instrument optimization, easily
250 obtains quantitative and qualitative data [12].

251 In this study, the animal model of chronic atrophic gastritis was mainly prepared by MNNG
252 combined with ammonia-free drinking water and hunger and satiety. The process of MNNG
253 alkylating the DNA bases does not depend on enzymatic metabolism and can directly penetrate
254 into the pylorus and stomach to cause canceration [13]. Alcohol can trigger acute ischemic damage
255 to the gastric mucosa, causing damaged genes to fail to recover over time, which may be an
256 important factor for initiating oncogenes [14]. Moreover, alcohol can accelerate the dissolution of
257 MNNG and increase the mutation rate. Ammonia can simulate toxic damage to the stomach after
258 *Helicobacter pylori* infection and maintain acute inflammation of the gastric mucosa [15,16].
259 Ranitidine hydrochloride can inhibit gastric acid secretion, but hunger and satiety are the fusion of
260 spleen and stomach damage. CAG is a complex disease with multiple factors and multiple genes.
261 Compound factor modeling can simulate human disease characteristics to a greater extent and is
262 currently the most widely used and most mature CAG model application.

263 Through PCA, PLS-DA and OPLS-DA LC-MS diversified analysis, using statistics,
264 bioinformatics, chemometrics and other methods to analyze and compare the differential
265 metabolites, the model group and the blank group of rat urine had significant metabolic
266 differences. A total of 68 different metabolites were screened, and 23 metabolic disturbance
267 pathways were predicted. The metabolic pathways can regulate the growth, differentiation,
268 apoptosis and the immune system of tumor cells [17]. The statistically significant metabolic

pathways are D-glutamine and D-glutamic acid metabolism, histidine metabolism, and purine metabolism. Among the metabolic pathways, the significantly different metabolites included L-glutamic acid and 10 different products, including ketoglutaric acid, histidine, 3-methyl-L-histidine, adenosine monophosphate, adenosine, adenine, hypoxanthine, guanosine and guanine.

L-Glutamic acid, which is in the metabolic pathway of D-glutamine and D-glutamic acid, plays an important role in protein metabolism in organisms. Studies have found that L-glutamic acid can inhibit cerebral cortex, hippocampal, gastric cancer cell and neural stem cell proliferation and differentiation and induce apoptosis [18,19]. Decreased glutamate expression levels will cause digestive system diseases. Based on this performance, L-glutamic acid is a commonly used therapeutic drug for the digestive system, especially gastric cancer and pancreatic cancer. Penicillin can induce the generation of glutamic acid and upregulate cycle-related expression genes and sugar degradation process of glucose to 2-oxoglutaric acid [20].

In the histidine metabolism pathway, 3-methyl-L-histidine, histidine, and L-glutamic acid play the role of substrate, intermediate, and product, respectively, and protein nutrition comes from the content of 3-methyl-L-histidine. Each of these compounds are effective indicators of histidine metabolic status [21]. Studies have confirmed that histidine can inhibit the proliferation and migration of lung cancer cells, thereby exerting an antitumor effect [22]. Histamine formed after the decarboxylation of histidine can relax blood vessels and is associated with inflammation. In gastritis and in the duodenum, the reaction in ulcers is sensitive. Currently, histidine is mostly used for the treatment of reducing gastric acid, relieving gastrointestinal pain and as a blood pressure

289 treatment. L-Glutamic acid is formed after a series of processes, such as phosphoester and propionic
290 acid formation, and its antagonists can reverse the abnormal expression of mGlu R5 and PSD-95 in
291 the striatum of LID rats [23].

292 Purine metabolism provides cells with the necessary energy and cofactors to promote the
293 growth and proliferation of cells. The most common disease with purine dysfunction is gout, and
294 purine metabolism and its metabolites include adenosine monophosphate, adenosine, adenine, and,
295 at times, the abnormal expression of xanthine, guanosine and guanine will promote the occurrence
296 of gastric cancer [24]. The decomposition of purine nucleotides will promote the
297 dephosphorylation of inosine or guanylic acid and generate inosine or guanosine, which can
298 decompose into xanthine or guanine. The CN-II enzyme is highly expressed in tumor cells [25].
299 Studies have shown that purine nucleotides are essential for metabolic functions. Hypoxanthine,
300 guanine phosphoribosyl transferase and other related purines can affect hematopoietic stem cell
301 cycle progression, proliferation kinetics and changes in mitochondrial membrane potential [26].
302

303 # Conclusions

304 Metabolomics is an important technical means for studying the pathogenesis of diseases.
305 This experiment is the first to use LC-MS metabolomics to study the pathogenesis of CAG from
306 the perspective of urine metabolites. Fromm the method (PCA) and supervised analysis method
307 (PLS-DA and OPLS-DA), differential metabolites of the model group and the control group were
308 screened. These differences were mainly distributed among 23 metabolic pathways, which were

309 glutamine metabolism with L-glutamic acid, 2-ketoglutarate in the D-glutamic acid metabolism
310 pathway, 3-methyl-L-histidine, histidine, L-glutamic acid and purine in the histidine metabolism
311 pathway. Adenosine monophosphate, adenosine, adenine, inosine, guanosine and guanine may be
312 potential biomarkers for the diagnosis of CAG.
313

## 314 Acknowledgments

315 The authors thank Suzhou BioNovoGene Biopharmaceutical Technology Co., Ltd., for their
316 technical assistance.And the Editing and Manuscript Formatting service provided by American
317 Journal Experts
318

# References

1. Jiang Y, Qi X, Liu X, Zhang J, Ji J, Zhu Z, et al. Fbxw7 haploinsufficiency loses its protection against DNA damage and accelerates MNU-induced gastric carcinogenesis. Oncotarget. 2017;8: 33444-33456.
2. Hao H. Correlation between pathological classification of chronic atrophic gastritis patients and TCM constitution types. Shanxi Provincial Institute of Traditional Chinese Medicine; 2017.
3. Wu Q. CKD-MBD related biomarkers based on metabolomics biological screening and research on the toxicity mechanism of bone metabolism. Second Military Medical University; 2017.
4. Hu T. Research on new methods and strategies for the analysis of endogenous lipid compounds based on chromatographic mass spectrometry. Peking Union Medical College; 2018.
5. Kong XR, Yang Y, Li HZ, Liu L, Zhao SM, Liu HY, et al. The effect of different routes and doses of N-methyl-N-nitro N-nitrosoguanidine administration on pathological changes of gastric mucosa in rats. Chin J Integr Tradit West Med Dig. 2015;23: 381-384, 389.
6. Want EJ, Masson P, Michopoulos F, Wilson ID, Theodoridis G, Plumb RS, et al. Global metabolic profiling of animal and human tissues via UPLC-MS. Nat Protoc. 2013;8: 17-32.

7. Smith CA, Want EJ, O'Maille G, Abagyan R, Siuzdak G. XCMS: processing mass spectrometry data for metabolite profiling using nonlinear peak alignment, matching, and identification. Anal Chem. 2006;78: 779-787.
8. Zhao F, et al. Liquorice aqueous extract intervenes in the liver metabolomics of D-galactose-induced aging rats. Chin Herb Med. 2017;48: 3545-3553.
9. Bai Z, Che Y. Application of BP neural network based on PCA in information security. Electron Technol Softw Eng. 2019;206-207.
10. Li WX, Wang XY, Tang JF, Zhang SQ, Wang Y, Zhang H, et al. Comparative study on the effect of Danggui-Chuanxiong herb pair on vasoactive substances and adhesion molecules in the serum of acute blood stasis in rats using PLS-DA and multi-attribute comprehensive index methods. Acta Pharm Sin. 2019;54: 1909-1917.
11. Xia J, Wishart DS. MetPA: a web-based metabolomics tool for pathway analysis and visualization. Bioinformatics. 2010;26: 2342-2344.
12. Pitt JJ. Principles and applications of liquid chromatography-mass spectrometry in clinical biochemistry. Clin Biochem Rev. 2009;30: 19-34.
13. Qi X, et al. Experimental study on the effect of MNNG compound method on the model of gastric precancerous lesions on inflammatory factors. Hubei J Tradit Chin Med. 2019;41: 3-4.
14. Yuan X. Research progress of rat models of precancerous lesions. J Anhui Tradit Chin Med Coll. 2004;23: 62-64.

15. Si J, Wu J, Cao Q, Zun JL. Establishment of rat model of chronic atrophic gastritis discussion on the factors of atrophy. Chin J Dig. 2001: 7-10.

16. Geng Z, Huang Y, Chen J. Experimental study on the effect of Taibai rice n-butanol extract on chronic gastritis in rats. Jilin Zhong Med. 2009;29: 527-528.

17. Wei J, Wu A, Kong LY, Wang Y, Fuller G, Fokt I, et al. Hypoxia potentiates glioma-mediated immunosuppression. PLoS One. 2011;6: e16195.

18. Gao C, Wang J, Zhou X. Changes of neuronal apoptosis in rat model of kidney yin deficiency induced by L-monosodium glutamate. Chin J Med. 2003: 719-720.

19. Gao S, Wang J. Changes of neural stem cell proliferation and differentiation-related proteins in L-monosodium glutamate rats. J Third Mil Med Univ. 2004: 1524-1526.

20. Hirasawa T, Saito M, Yoshikawa K, Furusawa C, Shmizu H. Integrated analysis of the transcriptome and metabolome of corynebacterium glutamicum during penicillin-induced glutamic acid production. Biotechnol J. 2018;13: 1700612.

21. Chen D, et al. Amino acid analyzer for rapid determination of 3-methylhistidine in urine. Sichuan J Physiol Sci. 1988: 56-57.

22. Escobar-Reséndiz R, Reyes-Esparza J, Blake IO, Rodriguez-Fragoso L. Evaluation of antitumoral effect of the combination of L-histidine methyl esther hydrochloride of anfotericin B with antineoplastics on A549 cells. FASEB J. 2020;34: 1.

376 23. Shu H. Experimental study on the effect of metabolic glutamate receptor 5 antagonist
377 MPEP on rats with levodopa-induced Parkinson's disease dyskinesia. Suzhou University;
378 2015.
379 24. Feng X, Ma D, Zhao J, Song Y, Zhu Y, Zhou Q, et al. UHMK1 promotes gastric cancer
380 progression through reprogramming nucleotide metabolism. EMBO J. 2020;39: e102541.
381 25. Tozzi MG, Pesi R, Allegrini S. On the physiological role of cytosolic 5'-nucleotidase II
382 (cN-II): pathological and therapeutical implications. Curr Med Chem. 2013;20: 4285-4291.
383 26. Vogel M, Moehrle B, Brown A, Eiwen K, Sakk V, Geiger H. HPRT and purine salvaging
384 are critical for hematopoietic stem cell function. Stem Cells. 2019;37: 1606-1614.
385

# Supporting information

S1 Fig. Mass Variation Diagram of the Control Group and Model Group.

S2 Fig. HE Staining Pathological Sections. A. HE Staining Pathological Sections of Gastric Mucosa in the Control Group (×200); 2-B: HE Staining Pathological Sections of Gastric Mucosa in the Model Group (×200).

S3 Fig. Chromatogram in Total Ion Mode. 3-A: Typical Sample BPC in Positive Ion Mode, 3-B: Typical Sample BPC in Negative Ion Mode.

S4 Fig Urine Metabolism Profile of CAG Model Rats in Positive Ion Mode. 4-A: PCA Scores, 4-B: PLS-DA Scores, 4-C: OPLS-DA Scores, 4-D: Replacement Test of the CAG Model Urine Fit Model in Positive Ion Mode.

S5 Fig Urine Metabolism Profile of CAG Model Rats in Negative Ion Mode. 5-A: PCA Scores, 5-B: PLS-DA Scores, 5-C: OPLS-DA Scores, 5-D: Replacement Test of the CAG Model Urine Fit Model in Negative Ion Mode.

S6 Fig Heat Map of the Differential Metabolites. A: Heat Map of the Differential Metabolites in CAG Rats; 6-B: Correlation Heat Map of Differential Metabolites in CAG Rats.

S7 Fig Metabolic Pathways of CAG Rat Metabolites Mapped to KEGG.